

Skin effect in neutron transport theory

E. L. Gaggioli^{*} and D. M. Mitnik

Instituto de Astronomía y Física del Espacio (IAFE, CONICET-UBA), Casilla de Correo 67 - Suc. 28 (C1428ZAA), Buenos Aires, Argentina

O. P. Bruno

Computing and Mathematical Sciences, California Institute of Technology, Pasadena, California 91125, USA



(Received 25 February 2021; accepted 1 September 2021; published 20 September 2021)

We identify a neutron-flux “skin effect” in the context of neutron transport theory. The skin effect, which emerges as a boundary layer at material interfaces, plays a critical role in a correct description of transport phenomena. A correct accounting of the boundary-layer structure helps bypass computational difficulties reported in the literature over the last several decades, and should lead to efficient numerical methods for neutron transport in two and three dimensions.

DOI: [10.1103/PhysRevE.104.L032801](https://doi.org/10.1103/PhysRevE.104.L032801)

The physical character of the neutron fluxes within and around heterogeneous materials, for given sources, has been the subject of significant literature over the last 70 years [1–7]. Much of this literature has been devoted to unraveling the complex interactions that result from the combined effect of neutron collision and transport phenomena [2–5]. This Letter describes and analyzes a physical observable, namely, a neutron-flux “skin effect” near physical boundaries, wherein sizable neutron fluxes exist for *incoming directions* nearly parallel to the boundary even in cases in which the exterior region is a source-free vacuum. The skin effect impacts in a significant way the simulation of nuclear reactors, and, as it concerns neutron fluxes that are nearly tangential to the boundary (which can eventually cross curved boundaries), it provides a useful system state indicator affecting reactor shielding and control as well as design and optimization [8,9].

The boundary skin effect under consideration arises as neutrons may travel for relatively long distances near the material-vacuum boundary along paths approximately parallel to the boundary, and can thus create significant neutron fluxes for *incoming directions* at material points *arbitrarily close to the boundary*—even when, for the vacuum-enclosed systems considered, the incoming fluxes *at the material boundary* vanish exactly. The geometrical context can be easily visualized in Fig. 1 for the flat-boundary case considered in this Letter, but such long neutron paths exist near curved boundaries as well.

Mathematically, the skin effect is encapsulated in sharp “boundary-layer” structures of the type described in Chap. 9 in Ref. [10] and detailed below. Albeit present in, e.g., eigenfunction solutions for neutron transport problems in one-dimensional (see Chap. 4 in Ref. [2]) or separable configurations [6], these boundary-layer transitions, which lead to unbounded gradients arbitrarily close to the interface boundaries, need to be correctly accounted for and fully recognized.

A mathematical reformulation of the neutron transport problem via a combination of changes of variables for the spatial and angular variables is presented in this Letter, which facilitates the skin-effect analysis. In particular, this approach enables the accurate modeling of neutron fluxes at arbitrarily small distances from the domain boundary, and, therefore, everywhere in the combined angular-spatial domain.

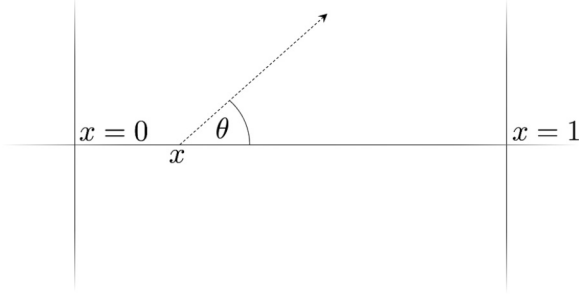
The equation for time-independent neutron transport in a one-dimensional plane-parallel geometry (Fig. 1), with isotropic scattering and vacuum boundary conditions, is given by [9,11]

$$\begin{aligned} \xi \frac{\partial}{\partial x} u(x, \xi) + \mu_t(x) u(x, \xi) &= \frac{\mu_s(x)}{2} \int_{-1}^1 u(x, \xi') d\xi' + q(x, \xi), \\ u(x = 0, \xi) &= 0 \quad \forall \xi > 0, \\ u(x = 1, \xi) &= 0 \quad \forall \xi < 0. \end{aligned} \quad (1)$$

Here, letting $\xi = \cos(\theta)$ (Fig. 1), and calling $\mu_s(x)$, $\mu_a(x)$, and $\mu_t(x) = \mu_a(x) + \mu_s(x)$ the macroscopic scattering, absorption, and total transport coefficients, respectively, $u(x, \xi)$ denotes the neutron flux at point x in the direction θ . The integral term accounts for the angular redistribution of neutrons due to scattering, $q(x, \xi)$ is a neutron source, and the vacuum boundary conditions model the absence of particles entering the spatial domain through its boundary. It is worthwhile noting that Eq. (1) also governs the transport of photons and other neutral particles, and it therefore impacts upon a wide range of important disciplines [2,3,6,12–23].

Noting that the coefficient ξ of the highest-order derivative in (1) tends to zero as $\theta \rightarrow \pi/2$, the existence of unbounded spatial gradients at points (x, ξ) near $(0,0)$ and $(1,0)$ in the solution $u(x, \xi)$ may be expected (see Chap. 9 in Ref. [10]). Such “boundary-layer” structures, which are caused by the existence of a spatial boundary condition in conjunction with a vanishingly small coefficient for the highest-order differential

*egaggioli@iafe.uba.ar

FIG. 1. One-dimensional finite “slab” geometry: $\xi = \cos(\theta)$

operator, only take place for the incoming directions $\xi > 0$ ($\xi < 0$) for points close to $x = 0$ ($x = 1$)—since it is for such directions that boundary conditions are imposed in Eq. (1).

Following Ref. [10] (see Chap. 9 therein), in order to characterize the boundary-layer structure around, e.g., $x = 0$, we consider the function $U(X, \xi) = u(\xi X, \xi)$ and, more precisely, its lowest-order asymptotics $U_0(X, \xi)$ as $\xi \rightarrow 0^+$ in a small neighborhood of the boundary (the boundary layer around $x = 1$ can be treated analogously). The function $U_0(X, \xi)$ (the *inner solution* in the nomenclature of Ref. [10], Chap. 9) satisfies the *constant coefficient* equation

$$\begin{aligned} \frac{\partial U_0(X, \xi)}{\partial X} + \mu_t(0)U_0(X, \xi) \\ = \frac{\mu_s(0)}{2} \int_{-1}^1 U_0\left(\frac{\xi X}{\xi'}, \xi'\right) d\xi' + q(0, \xi), \end{aligned} \quad (2)$$

and boundary conditions induced by (1). Equation (2) tells us that the derivative $\frac{\partial U_0(X, \xi)}{\partial X}$ remains bounded as $\xi \rightarrow 0^+$, and, therefore, that the function $U_0(X, \xi)$ characterizes the boundary-layer structure in the solution $u(x, \xi)$ via the relation

$$u(x, \xi) \sim u_0(x, \xi) = U_0(x/\xi, \xi) \quad \text{as } (x, \xi) \rightarrow (0^+, 0^+). \quad (3)$$

Utilizing an integrating factor in (2) and letting

$$I(x, \xi) = \int_0^x e^{\frac{\mu_t(0)y}{\xi}} \left[\frac{\mu_s(0)}{2} \int_{-1}^1 u_0(y, \xi') d\xi' + q(0, \xi) \right] dy,$$

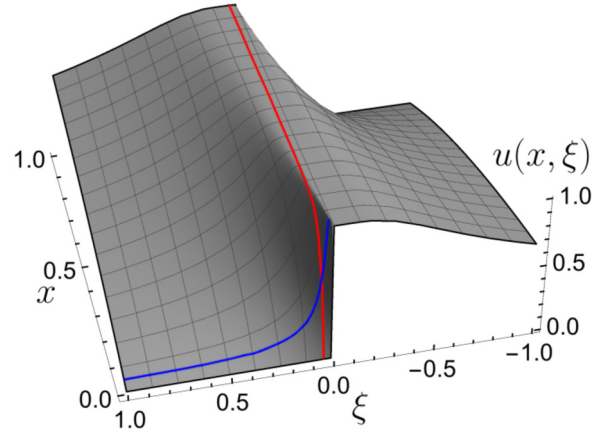
the lowest-order boundary-layer approximation

$$u(x, \xi) \sim u_0(x, \xi) = \frac{e^{-\mu_t(0)x/\xi}}{\xi} I(x, \xi) \quad (4)$$

is obtained. This equation explicitly exhibits the exponential boundary-layer character of the solution. The argument can be extended to two- and three-dimensional (2D and 3D) problems, and to include time-dependence and curved boundaries. In such cases, a boundary layer occurs, with unbounded normal derivatives near the boundary, for incoming directions nearly parallel to the domain interface.

The boundary-layer structure can be visualized by considering the exact solution of Eq. (1) that is obtained for the scattering-free case [$\mu_s(x) = 0$] with constant coefficients. The resulting solution,

$$u(x, \xi) = \begin{cases} \frac{q}{\mu_a} [1 - e^{-\mu_a x/\xi}] & \forall \xi > 0, \\ \frac{q}{\mu_a} [1 - e^{-\mu_a(x-1)/\xi}] & \forall \xi < 0, \end{cases} \quad (5)$$

FIG. 2. Scattering-free solution [Eq. (5)]. The boundary layers in the ξ and x directions are clearly emphasized by the superimposed blue (along the ξ direction) and red (along the x direction) coordinate curves.

presented in Fig. 2, clearly displays a boundary-layer structure as $(x, \xi) \rightarrow (0^+, 0^+)$.

The skin effect significantly impacts the mathematical modeling of neutron transport processes. The foremost two numerical methods used in the area, namely, the spherical harmonics method (see Ref. [2] and Chap. 8 therein) and the discrete ordinates method (see Ref. [3] and Chaps. 3 and 4 therein), do not properly resolve the conflicting manifestations of the skin effect in the angular and spatial variables (see pp. 65 and 66 in Ref. [5]), leading to significant degradations in accuracy [24–26] (see p. 51 in Ref. [27]). Most conspicuously, Ref. [4] (see p. 40 therein) shows that different numerical differentiation schemes may lead to different numerical solutions. It has been demonstrated that, for separable geometries, a degree of accuracy can be obtained for certain spatial “region averages” of the “angular average” of the neutron flux [6,7,12]; naturally, however, general domains are not separable, and, in addition, the full neutron flux (not just such multiply averaged quantities) is generally required for detector response calculations (see p. 60, problem 1–13 in Ref. [3] and Sec. 6.4.3 in Ref. [28]).

A combination of spatial and angular changes of variables can be used to eliminate the difficulties posed by the dual spatial/angular boundary layers. To introduce the angular change of variables we rely on the Gauss-Legendre method as an underlying quadrature rule, but other quadrature methods could alternatively be used. In view of the expression on p. 77 in Ref. [29], the ℓ -point Gauss-Legendre quadrature error decreases as $32V/15\pi j(2\ell + 1 - j)^j$ provided the $j \leq 2\ell$ derivative of the integrated function is bounded by the constant $V > 0$. Introducing the change of variables $\xi' = r^p$ in the integral in (1) we thus seek a bound V on the j th derivative of the resulting integrand. Using an integrated version of (1), similar to (4), combining two exponential terms, and using the fact that for each non-negative integer k the integral $\int_0^\infty t^k e^{-t} dt$ is finite, we find that

$$\left| \frac{\partial^j}{\partial r^j} [u(x, r^p) r^{p-1}] \right| \leq W r^{p-j-1} \quad (6)$$

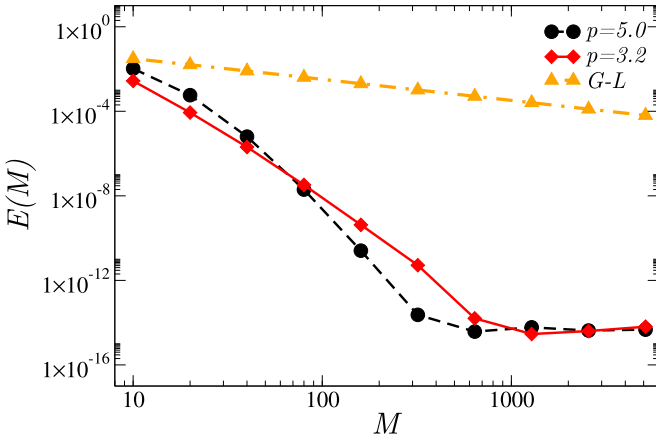


FIG. 3. Error of numerical against analytic integral, $E(M) = \max_{0 \leq x \leq 1} |\sum_{i=1}^M w_i u(x, \xi_i) - I^{\text{an}}(x)|$, for u given by Eq. (5). The errors are presented for the quadrature rule (7) (circles and diamonds) and the plain Gauss-Legendre (GL) quadrature (triangles).

for some constant W [even as $(x, r) \rightarrow (0^+, 0^+)$]; setting $V = Wr^{p-j-1}$ yields the desired bound, which, importantly, is uniform for all relevant values of x and r (as long as $p \geq j + 1$).

Splitting the integral on the right-hand side of Eq. (1) at the boundary-layer point $\xi = 0$ and using the proposed change of variables yields

$$\int_0^1 u(x, \xi) d\xi \sim \sum_{i=1}^{M/2} w_i u(x, \xi_i), \quad (7)$$

with a similar expression for the integral between -1 and 0 . Here, letting r_i and w_i^{GL} denote the Gauss-Legendre quadrature abscissas and weights in the interval $[0, 1]$, we have set $\xi_i = r_i^p$ and $w_i = p \times r_i^{p-1} \times w_i^{\text{GL}}/2$. A suitable power $p = 3.2$ was used, which provides excellent convergence (Fig. 3) for the integral in the ξ variable while limiting the sharpness of the numerical boundary layer in the x variable.

The logarithmic spatial change of variables $v = \log(\frac{x}{1-x})$, in turn, is used to resolve the spatial boundary layer, which gives rise to points x extremely close to the boundary [without detriment to the integration process, in view of the *uniform-derivative* bounds (6)], leading to high-order precision in both the ξ and x variables. If the change of variables $\xi' = r^p$ were not introduced, then finer and finer angular discretizations, without a bound on the number of angular discretization points used, would be necessary to yield a fixed prescribed accuracy as the spatial point x approaches a boundary point. Similarly, the logarithmic change of variables allows for the resolution of the rapid changes in the angular flux arising from the spatial boundary layer near the boundaries.

The transport equation is solved in a computational spatial domain $[v_{\min}, v_{\max}]$, with $[x'_{\min}, x'_{\max}] = [\frac{e^{v_{\min}}}{e^{v_{\min}}+1}, \frac{e^{v_{\max}}}{e^{v_{\max}}+1}]$, and with boundary conditions at x'_{\min} and x'_{\max} obtained by enforcing the asymptotic relation (4) with $u_0(y, \xi')$ replaced by $u_0(x'_{\min}, \xi')$ and $u_0(x'_{\max}, \xi')$, respectively. Using the new

variables the time-dependent transport problem,

$$\frac{\partial}{\partial t} u(v, \xi, t) + \xi [2 + 2 \cosh(v)] \frac{\partial}{\partial v} u(v, \xi, t) + \mu_t u(v, \xi, t) = \frac{\mu_s}{2} \int_{-1}^1 u(v, \xi', t) d\xi' + q, \quad (8)$$

$$u(v, \xi, t_{\min}) = 0,$$

$$u(v_{\min}, \xi, t) = u_0(x'_{\min}, \xi, t) \quad \forall \xi > 0,$$

$$u(v_{\max}, \xi, t) = u_0(x'_{\max}, \xi, t) \quad \forall \xi < 0$$

results. The time propagation is performed implicitly by means of a third-order backward differentiation formula (BDF). The collisional term is obtained by means of the third-order polynomial extrapolation $\tilde{u}_j^{n+1} = \sum_{\kappa=0}^2 (-1)^\kappa \binom{3}{\kappa+1} u_j^{n-\kappa}$ [see Eq. (12) in Ref. [30]], to avoid the inversion of large matrices at each time step. Using the identity operator $\hat{\mathbb{I}}$ and the Fourier continuation (FC) spectral differentiation operator $\hat{\mathbb{D}}$ [31–33], the resulting discrete version of Eq. (8), which amounts to an implicit version of the FC discrete ordinates (FC-DOM) method [33], thus reads

$$\begin{aligned} & [\hat{\mathbb{I}} + \beta \Delta t \xi_j (2 + 2 \cosh(v)) \hat{\mathbb{D}} + \beta \Delta t \mu_t \hat{\mathbb{I}}] u_j^{n+1} \\ &= \sum_{k=0}^2 \alpha_k u_j^{n-k} + \beta \Delta t \frac{\mu_s}{2} \sum_{i=1}^M w_i \tilde{u}_i^{n+1} + \beta \Delta t q^{n+1}, \end{aligned} \quad (9)$$

where $u_j^{n+1} \sim u(v, \xi_j, t^{n+1})$, $t^{n+1} = n\Delta t$, and where α_k and β are the coefficients for the third-order BDF formula. (The FC method enables representation of general smooth nonperiodic functions by a Fourier series while avoiding the well-known Gibbs ringing phenomenon, with applicability to the solution of partial differential equations in general multidimensional spatial domains with high accuracy and negligible numerical dispersion [31–33].) Figure 4 demonstrates the excellent convergence properties of the algorithm, for $\mu_s = \mu_a = q = 1$. The error was computed via comparison with the solution obtained on a finer grid. This high order of convergence clearly suggests that the changes of variables used in the x and ξ variables lead to an adequate simultaneous grid resolution of the two boundary layers involved.

In what follows, the numerical algorithm is utilized to explore and demonstrate the skin effect. For definiteness, in the rest of this Letter we restrict attention to time-independent solutions, obtained by means of the time-dependent solver, relaxed for long times (as described in Ref. [33]). The resulting steady-state solutions are depicted in various forms in Figs. 5–7; similar boundary-layer structures are of course present for all times in the time-dependent solutions. Figure 5 displays the skin-effect boundary-layer structures in the x and ξ variables with $\mu_s = \mu_a = q = 1$ (numerical parameter values $N = 250$ and $M = 40$ were used in these figures, with $-v_{\min} = v_{\max} = 25$). As can be seen in Fig. 5, as ξ decreases towards zero, steeper and steeper boundary layers result, over shrinking spatial regions, as expected from the proposed boundary-layer analysis—thus giving rise to large nearly boundary-parallel incoming neutron fluxes in close proximity to the boundaries.

Figure 6 demonstrates the persistence of the boundary layer in the presence of high scattering coefficients (with

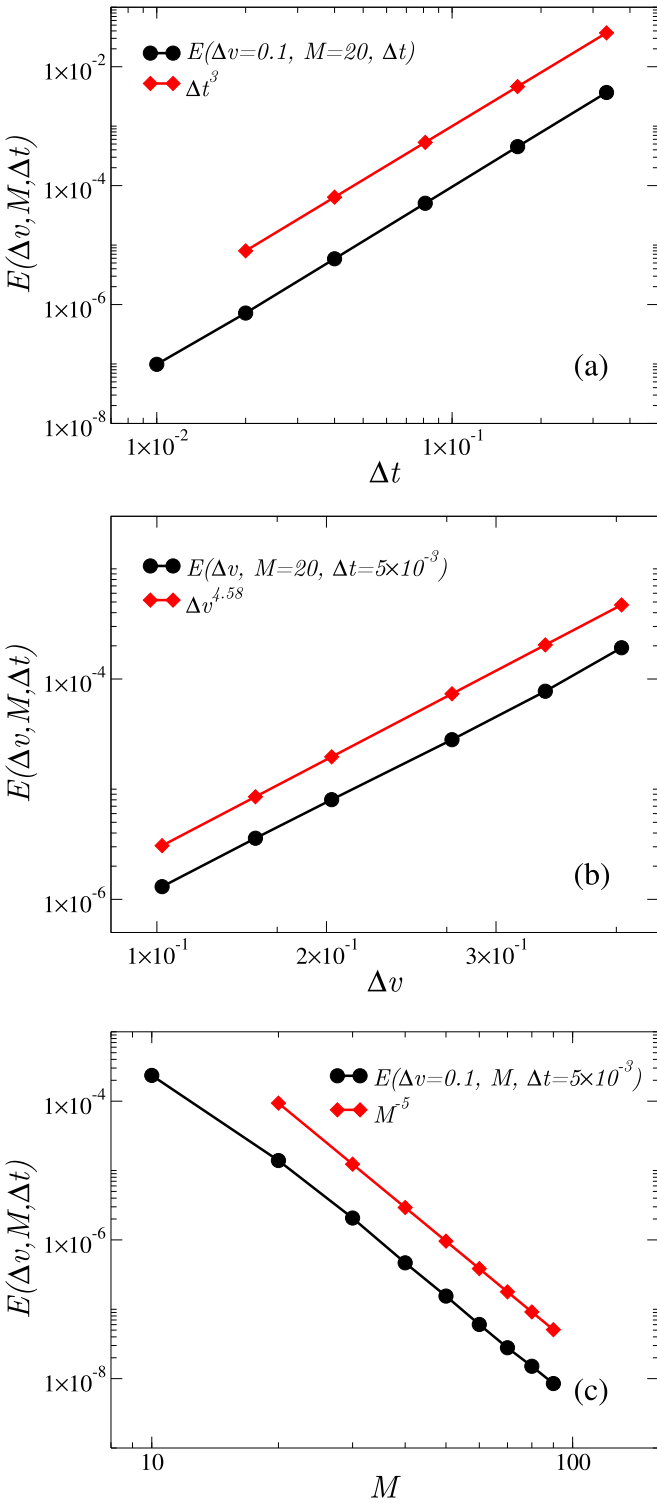


FIG. 4. Convergence properties of the proposed algorithm for (a) the time discretization, (b) the spatial discretization, and (c) the number of discrete ordinates employed. In circles, the error $E(\Delta v, M, \Delta t) = \max_{x, \xi} |u(x, \xi) - u^c(x, \xi)|$ is displayed for various grids, where $u^c(x, \xi)$ denotes the converged solution.

$\mu_a = q = 1$ fixed). The case $\xi = \xi_{\min} \simeq 10^{-6}$ is considered in the figure, with parameter values $N = 200$, $M = 20$, and $-v_{\min} = v_{\max} = 20$. Clearly, even though diffusive problems (large μ_s) tend to be more regular over the ξ variable—owing

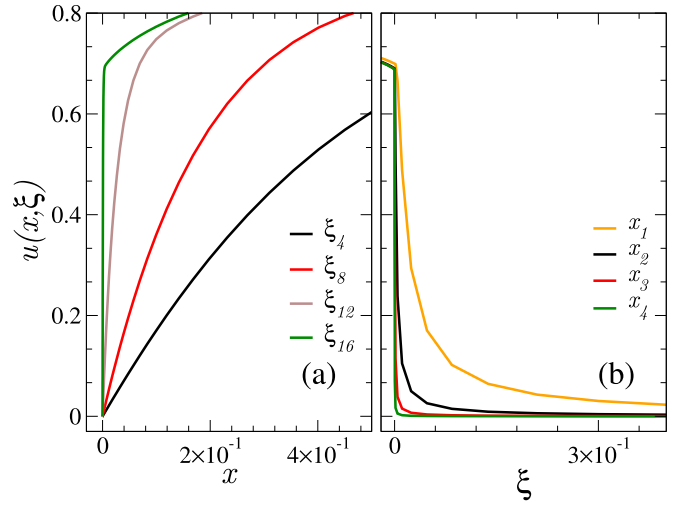


FIG. 5. Boundary layers near $x = 0$, obtained by solving Eq. (8) with $\mu_a = \mu_s = q = 1$ for various values of ξ and x , with $0.84 > \xi_i > \xi_{i+1} > 10^{-7}$ and $10^{-2} > x_i > x_{i+1} > 10^{-6}$. (a) shows the boundary layer along the x variable for various values of ξ , and (b) shows the boundary layers along the ξ variable for various values of x . The neutron flux $u(x, \xi)$ does not vanish on the boundary for the outgoing directions $-1 \leq \xi < 0$, and, therefore, no boundary layer exists at $x = 0$ for such directions (not shown).

to the strong averaging and smoothing induced by the large scattering coefficient—the boundary layers that arise in the spatial variable with increasing μ_s lead to even larger slopes as $x \rightarrow 0^+$.

There have been many attempts to understand unphysical oscillations associated with the widely used diamond difference scheme (DD) for the transport equation [4,34,35]. A recent paper [24] avoids this problem by using only directions ξ away from $\xi = 0$. References [4,34] attribute these types of oscillations to anisotropic boundary conditions, nondiffusive boundary layers, and/or high absorption; the present Letter, which demonstrates the existence of boundary layers

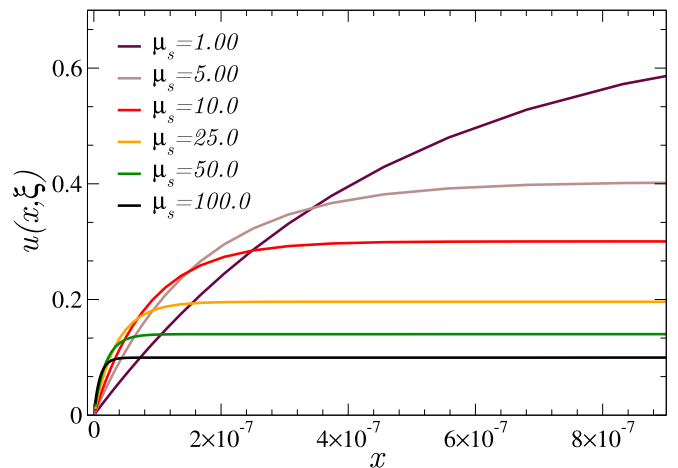


FIG. 6. Boundary layers obtained by solving Eq. (8), with $\mu_a = q = 1$ and different values of μ_s . Solutions for the direction $\xi = \xi_{\min} \simeq 10^{-6}$ are shown. Note the large μ_s -dependent slopes of the transport solution as $x \rightarrow 0^+$ [cf. Eq. (4), where $\mu_t = \mu_s + \mu_a$].

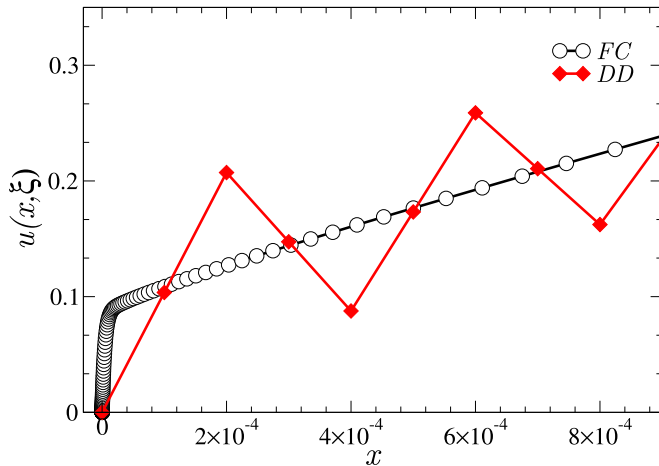


FIG. 7. DD and FC-DOM approximations of $u(x, \xi_{15})$ for $\mu_t = \mu_s = 1000$, $q = 0.1$, and $\xi_{15} \simeq 10^{-3}$. The boundary-layer oscillations resulting from the DD scheme are clearly visible. $N = 400$ and $N = 10\,000$ discrete points were used in the spatial variable for the FC and DD methods, respectively. Note the high near-boundary resolution that results, in view of the exponential spatial change of variables used, from the $N = 400$ FC-DOM discretization.

even in the isotropic case and for all values of the scattering and absorption coefficients, presents a starkly contrasting interpretation: Exponential boundary layers are triggered by the boundary condition and vanishing ξ values. For example, Ref. [34] treats a diffusive transport problem (problem 1 in that reference) which, under rescaling, can be reformulated as in Eq. (1) with $\mu_s = \mu_t = 1000$, and $q = 0.1$. This is an extremely diffusive problem with isotropic boundary

conditions for which Ref. [34] (see p. 317 therein) states “...since the leading order term in the asymptotic expansion of the analytic transport equation is itself isotropic, this term in these problems does not contain a boundary layer.” In contrast, Fig. 7 shows that boundary layers are present in this problem. The FC-DOM solution displayed in this figure was obtained by means of $M = 40$ discrete directions and $N = 400$ points in the spatial variable. In contrast, $N = 10\,000$ were used in the DD-scheme solution presented in Fig. 7—which clearly displays the spurious oscillations produced by the DD scheme in this context.

The skin-effect boundary-layer structure described in this Letter constitutes a physical effect which was overlooked for nearly 70 years (see p. 360 in Ref. [1] and p. 317 in Ref. [34]), and which, as demonstrated in Fig. 7 and throughout this Letter, has a significant impact on the physics and the numerical simulation of transport phenomena. In particular, this work provides a sound theoretical basis for the development of accurate and efficient methods for the numerical solution of neutron transport and other neutral particle-transport problems, in general 2D and 3D domains, and it leads to valuable state indicators concerning reactor dynamics.

O.P.B. was supported by NSF through Contract No. DMS-1714169 and by the NSSEFF Vannevar Bush Fellowship under Contract No. N00014-16-1-2808. E.L.G. and D.M.M. gratefully acknowledge the financial support from the following Argentine institutions: Consejo Nacional de Investigaciones Científicas y Técnicas (CONICET), PIP 11220130100607, Agencia Nacional de Promoción Científica y Tecnológica (ANPCyT) PICT-2017-2945, and Universidad de Buenos Aires UBACyT 20020170100727BA.

- [1] S. Chandrasekhar, *Radiative Transfer*, 1st ed. (Clarendon, London, 1950).
- [2] K. M. Case and P. F. Zweifel, *Linear Transport Theory*, 1st ed. (Addison-Wesley, Reading, MA, 1967).
- [3] E. E. Lewis and W. F. Miller, *Computational Methods of Neutron Transport*, 1st ed. (Wiley, New York, 1984).
- [4] B. G. Petrović and A. Haghghat, Analysis of inherent oscillations in multidimensional S_N solutions of the neutron transport equation, *Nucl. Sci. Eng.* **124**, 31 (1996).
- [5] B. Hunter and Z. Guo, Numerical smearing, ray effect, and angular false scattering in radiation transfer computation, *Int. J. Heat Mass Transfer* **81**, 63 (2015).
- [6] L. B. Barichello, A. Tres, C. B. Picoloto, and Y. Y. Azmy, Recent studies on the asymptotic convergence of the spatial discretization for two-dimensional discrete ordinates solutions, *J. Comput. Theor. Transp.* **45**, 299 (2016).
- [7] X. Hu and Y. Y. Azmy, Asymptotic convergence of the angular discretization error in the scalar flux computed from the particle transport equation with the method of discrete ordinates, *Ann. Nucl. Energy* **138**, 107199 (2020).
- [8] A. Rodríguez Hernández, A. M. Gómez-Torres, and E. Del Valle-Gallegos, Nuclear reactor simulation, in *New Trends in Nuclear Science*, edited by N. S. Awwad and S. A. AlFaify (IntechOpen, London, 2018).
- [9] J. J. Duderstadt and L. J. Hamilton, *Nuclear-Reactor Analysis*, 1st ed. (Wiley, New York, 1976).
- [10] C. M. Bender and S. A. Orszag, *Advanced Mathematical Methods for Scientists and Engineers I*, 1st ed. (Springer, New York, 1999).
- [11] J. J. Duderstadt and W. R. Martin, *Transport Theory*, 1st ed. (Wiley, New York, 1979).
- [12] X. Hu and Y. Y. Azmy, On the regularity order of the pointwise uncollided angular flux and asymptotic convergence of the discrete ordinates approximation of the scalar flux, *Nucl. Sci. Eng.* **195**, 598 (2021).
- [13] A. D. Klose, U. Netz, J. Beuthan, and A. H. Hielscher, Optical tomography using the time-independent equation of radiative transfer - Part 1: Forward model, *J. Quant. Spectrosc. Radiat. Transfer* **72**, 691 (2002).
- [14] A. Corlu, R. Choe, T. Durduran, M. A. Rosen, M. Schweiger, S. R. Arridge, M. D. Schnall, and A. G. Yodh, Three-dimensional in vivo fluorescence diffuse optical tomography of breast cancer in humans, *Opt. Express* **15**, 6696 (2007).
- [15] K. Ren, Recent developments in numerical techniques for transport-based medical imaging methods, *Commun. Comput. Phys.* **8**, 1 (2010).
- [16] H. Fujii, K. Nadamoto, S. Okawa, Y. Yamada, M. Watanabe, Y. Hoshi, and E. Okada, Numerical modeling of photon

- migration in human neck based on the radiative transport equation, *J. Appl. Nonlinear Dyn.* **5**, 117 (2016).
- [17] O. N. Vassiliev, T. A. Wareing, J. McGhee, G. Failla, M. R. Salehpour, and F. Mourtada, Validation of a new grid-based Boltzmann equation solver for dose calculation in radiotherapy with photon beams, *Phys. Med. Biol.* **55**, 581 (2010).
- [18] J. Qin, J. J. Makela, F. Kamalabadi, and R. R. Meier, Radiative transfer modeling of the OI 135.6 nm emission in the nighttime ionosphere, *J. Geophys. Res., A: Space Phys.* **120**, 10116 (2015).
- [19] R. Siegel and J. R. Howell, *Thermal Radiation Heat Transfer*, 3rd ed. (Taylor and Francis, New York, 2001).
- [20] A. Badruzzaman, Computational methods in nuclear geophysics, *Prog. Nucl. Energy* **25**, 265 (1991).
- [21] J. Przybilla, M. Korn, and U. Wegler, Radiative transfer of elastic waves versus finite difference simulations in two-dimensional random media, *J. Geophys. Res.: Solid Earth* **111**, B04305 (2006).
- [22] E. G. Mishchenko and C. W. J. Beenakker, Radiative Transfer Theory for Vacuum Fluctuations, *Phys. Rev. Lett.* **83**, 5475 (1999).
- [23] R. Prasher, Generalized equation of phonon radiative transport, *Appl. Phys. Lett.* **83**, 48 (2003).
- [24] D. Wang and T. Byambaakhuu, High-Order Lax-Friedrichs WENO fast sweeping methods for the S_N neutron transport equation, *Nucl. Sci. Eng.* **193**, 982 (2019).
- [25] R. Harel, S. Burov, and S. I. Heizler, Asymptotic P_N approximation in radiative transfer problems, *J. Comput. Theor. Transp.* **50**, 390 (2021).
- [26] J. C. Chai, H. O. Lee, and S. V. Patankar, Ray effect and false scattering in the discrete ordinates method, *Numer. Heat Transfer, Part B* **24**, 373 (1993).
- [27] J. Rocheleau, An analytical nodal discrete ordinates solution to the transport equation in Cartesian geometry, Master's thesis, Ohio State University, 2020.
- [28] A. D. Klose, Radiative transfer of luminescence light in biological tissue, in *Light Scattering Reviews 4*, edited by A. A. Kokhanovsky, Springer Praxis Books (Springer, Berlin, 2009), Chap. 6, pp. 293–345.
- [29] L. N. Trefethen, Is Gauss quadrature better than Clenshaw-Curtis? *SIAM Rev.* **50**, 67 (2008).
- [30] O. P. Bruno and M. Cubillos, Higher-order in time “quasi-unconditionally stable” ADI solvers for the compressible Navier-Stokes equations in 2D and 3D curvilinear domains, *J. Comput. Phys.* **307**, 476 (2016).
- [31] N. Albin and O. P. Bruno, A spectral FC solver for the compressible Navier-Stokes equations in general domains I: Explicit time-stepping, *J. Comput. Phys.* **230**, 6248 (2011).
- [32] O. P. Bruno, M. Cubillos, and E. Jimenez, Higher-order implicit-explicit multi-domain compressible Navier-Stokes solvers, *J. Comput. Phys.* **391**, 322 (2019).
- [33] E. L. Gaggioli, O. P. Bruno, and D. M. Mitnik, Light transport with the equation of radiative transfer: The Fourier continuation - discrete ordinates (FC-DOM) method, *J. Quant. Spectrosc. Radiat. Transfer* **236**, 106589 (2019).
- [34] E. W. Larsen, J. E. Morel, and W. F. Miller, Asymptotic solutions of numerical transport problems in optically thick, diffusive regimes, *J. Comput. Phys.* **69**, 283 (1987).
- [35] G. Bal, Fourier analysis of diamond discretization in particle transport, *Calcolo* **38**, 141 (2001).